A Low-order Model of Two-dimensional Fluid Dynamics on the Surface of a Sphere

Mozheng Wei

CRC for Southern Hemisphere Meteorology, CSIRO Division of Atmospheric Research, Private Bag No.1, Mordialloc 3195, Australia

Received February 23; revised June 8, 1995

ABSTRACT

Without any other approximations apart from the spectral method which is employed, the energy spectra corresponding to two kinds of "negative temperatures" are simulated with a symmetric trapezium truncation. The simulated results with either of the two negative temperatures are reasonably consistent with those from the statistical theory of turbulence. The more usual case for two positive temperatures evolves differently from the theoretical prediction. The viscosity influence on the ergodicity is discussed. It is shown that two-dimensional (2D) ideal flows on the sphere have a less pronounced tendency to be ergodic than those on planar geometry due to the curvature of the spherical surface that weakens the interaction between different parts of the flow, enabling these parts to behave in more relative isolation. The expressions for the standard deviations from a canonical ensemble for the two different options of coefficients are shown to be proportional to $\sqrt{N}$ (N is the total number of independent modes in the system), independent of the initial conditions of the system.

Key words: Spectral method, Trapezium truncation, Negative temperature, Entropy, Enstrophy, ergodicity, Canonical ensemble, Generalized phase space

I. INTRODUCTION

Two-dimensional turbulence has been studied over many years (e.g. Batchelor, 1967 and 1969; Kraichnan, 1967 and 1975 etc.), mostly in the periodic Cartesian geometry. Numerical analysis has proved more popular and useful since the advent of powerful computers (e.g. Lilly, 1969 and 1971; Deem et al., 1971; Fox et al., 1973; Herring et al., 1974 and Seyler et al., 1975). Work by Brachet et al. (1988) presented some resolutions up to 800^2 for general periodic flows and 2048^2 for periodic flows with large symmetries. A transition of the inertial energy-spectrum exponent from $n \approx -4$ at early times to $n \approx -3$ when the turbulence becomes more mature was obtained by the authors.

In the spherical geometry, two-dimensional turbulence can model large scale long time atmospheric flows (over 100 km, Kraichnan et al., 1980) and some geophysical flows (e.g. Holloway, 1986). By using Fourier series and the pseudo-spectral method (Orszag, 1974), Tang and Orszag (1978) numerically showed that energy transfer is more local in spherical than in Cartesian geometry, so that there are weaker transfers to and from high mode numbers. The wavenumber cut-off they chose was 32. Frederiksen and Sawford (1980), in terms of spherical harmonics Y_m^n, derived the equilibrium kinetic energy and enstrophy spectrums by applying macrocanonical ensemble theory to the truncated spherical nondivergent barotropic equation which has been widely used as a nonlinear evolution equation for weather predictions. They compared the equilibrium results with numerical integrations initialized with the observed meteorological global fields. Different cut-offs for the rhomboidal truncations were used in their numerical procedures. They concluded that the small scales

tend to equilibrate more rapidly than the larger ones in the spherical situation as well as in the planar geometry (Fox and Orszag, 1973). Their numerical integrations were carried out on the basis of a set of concise one–level primitive equations, which was developed by Bourke (1972), incorporating the transform method proposed by Eliasen et al. (1970) and Orszag (1970). By utilizing spectral transform method, one can evaluate the nonlinear interaction term by transforming between the wave number space and a latitude–longitude grid at every time step, i.e. the multiplications in the nonlinear term can be carried out in grid space, the products can then be transformed back to the wave space. It has been this transform method that has greatly enhanced the efficiency and enlarged the capability of the spectral method so that the inherent advantages of the spectral method can be taken. Bourke et al. (1977) reviewed the development of the spectral models and the implementation of the spectral transform method.

In this paper, we concentrate on the numerical simulations of energy distributions over both wave numbers n and m in a particularly truncated Euler equation, without using any transform methods, any fast Fourier transforms or any approximate formulas for the spherical harmonics whatever. Because we do not use any simplifications in computing the nonlinear terms which transfer energy and enstrophy among the truncated wave numbers, the number of the expansions of each nonlinear component increases rapidly with increasing truncated wave numbers, $\sim N^5$ for large N (N is the cut–off number, see Orszag, 1970 and 1974 for details). A cut–off of $n=2\cdots7$ and $m=-n\cdots n$ is chosen. The nonlinear expressions in this truncation are still too long to be presented to the reader, even after some symmetries are imposed on the system. The results from pure numerical simulation are compared to those from absolute statistical mechanics treatment. We also report the calculations of the entropy in the three runs of this system. We use the definition of the entropy which was first suggested by Betchov (1964) to measure the degree of complication of a turbulent flow. This quantity offers a quantitative measure of the ergodicity of a system. For a ergodic system, the entropy increases rapidly and monotonically when it is far from the equilibrium state. The maximum value of the entropy appears when the system is in full equilibrium. On the other hand, the entropy evolution of a non–ergodic state displays huge fluctuations.

We briefly present our truncated system in Section 2. Before our numerical simulations are carried out in Section 4, this system is analysed by means of statistical theory of mechanics in Section 3. The ergodicity is studied in Section 5. Finally, we offer our remarks and discussions in Section 6.

II. THE MODEL OF THE TRUNCATED NAVIER–STOKES (EULER) EQUATION

We consider flows described by incompressible Navier–Stokes equations

$$\frac{\partial v}{\partial t}+v\cdot\nabla v=v\nabla^2 v-\nabla p, \tag{1}$$

$$\nabla\cdot v=0. \tag{2}$$

It is known that a two–dimensional non–divergent flow may be entirely described by a single scalar function of space and time (the stream function), which is denoted by $\psi(\theta,\ \varphi, t)$ in the case of spherical geometry. The sphere is assumed to be of unit radius in this paper. The stream function ψ can then be defined by

$$v=-\nabla\psi\times\mathbf{k}.$$

The vorticity field is given by $\xi=\nabla\times v=\nabla^2\psi\mathbf{k}$, the normal component of which (a scalar

function) is $\xi = \nabla^2\psi$ (where $\mathbf{k}$ is unit vector perpendicular to the surface of the sphere).

The stream function may be expanded in terms of spherical harmonics in order to solve the Euler equation using the spectral method

$$\psi(\theta,\varphi,t) = \sum_{n=n_1}^{n_2} \sum_{|m|\le n} a_n^m(t) Y_n^m(\theta,\varphi), \tag{3}$$

where the surface harmonic Y_n^m of degree n and order m is defined by

$$Y_n^m(\theta,\varphi) = \sqrt{\frac{(2n+1)(n-m)!}{4\pi \quad (n+m)!}} P_n^m(\cos\theta)\exp(im\varphi)$$

with $P_n^m(\cos\theta)$ which is the standard associated Legendre function. The reality of the stream function requires

$$a_n^{m*} = (-1)^m a_n^{-m}. \tag{4}$$

Hence we have our final truncated equations (a condition of $n \neq 0$ is assumed)

$$\dot{a}_n^m = N_n^m - \nu n(n+1) a_n^m \tag{5}$$

with

$$N_n^m = \frac{i(-1)^m}{n(n+1)} \sum_{n',n''=n_1}^{n_2} \sum_{|m'|,|m''|\le n_1,n_2} a_{n'}^{m'} a_{n''}^{m''} n''(n''+1)$$
$$C(n,n',n'') \begin{bmatrix} n-1 & n' & n'' \\ 0 & 0 & 0 \end{bmatrix} \begin{bmatrix} n & n' & n'' \\ -m & m' & m'' \end{bmatrix}, \tag{6}$$

where the dot denotes differentiation with respect to time t. Also

$$C(n,n',n'') = ((2n+1)(2n'+1)(2n''+1)(1+n+n'+n'')$$
$$(1+n'+n''-n)(n-n'+n'')(n+n'-n'')/(16\pi))^{1/2}$$

and $\begin{bmatrix} n & n' & n'' \\ -m & m' & m'' \end{bmatrix}$ is defined by the standard 3–j symbol (e.g. Jones, 1985).

The total kinetic energy E and enstrophy Ω per unit mass can be expressed in terms of the expansion coefficients of the stream function as below

$$E = \frac{1}{2}\oint_S v^2\,ds = \frac{1}{2}\oint_S (\nabla\psi)^2\,ds = \frac{1}{2}\sum_{n=n_1}^{n_2}\sum_{m=-n}^{n} n(n+1)\left|a_n^m\right|^2, \tag{7}$$

$$\Omega = \frac{1}{2}\oint_S \xi^2\,ds = \frac{1}{2}\oint_S (\nabla^2\psi)^2\,ds = \frac{1}{2}\sum_{n=n_1}^{n_2}\sum_{m=-n}^{n} n^2(n+1)^2\left|a_n^m\right|^2. \tag{8}$$

In general, viscosity causes the energy and the enstrophy to decrease with time.

$$\frac{dE}{dt} = \frac{1}{2}\frac{d}{dt}\oint_S (\nabla\psi)^2\,ds = -\frac{\nu}{2}\sum_{n=n_1}^{n_2}\sum_{m=-n}^{n} n^2(n+1)^2\left|a_n^m\right|^2 = -\nu\Omega.$$
$$\frac{d\Omega}{dt} = \frac{1}{2}\frac{d}{dt}\oint_S (\nabla^2\psi)^2\,ds = -\frac{\nu}{2}\sum_{n=n_1}^{n_2}\sum_{m=-n}^{n} n^3(n+1)^3\left|a_n^m\right|^2,$$

where S denotes the whole area of the spherical surface. The situation in the absence of external forces and viscosity will be considered first, so that the equations to be numerically solved

are

$$\dot{a}_n^m = N_n^m . \tag{9}$$

The spectral equations (9) along with expression (6) still conserve two quadratic constants of motion, which exist in the original inviscid Navier–Stokes equations. Here we have three points to make about the nonlinear terms N_n^m $(n = n_1 \cdots n_2$ and $m = -n \cdots n)$.

(i) $N_n^{m*} = (-1)^m N_n^{-m}$, (ii) $N_n^0 = 0$, (iii) $N_1^m = 0$.

(iii) tells us that the energy components E_1^m (with $m = -1,0,1$) are constants of motion. This is consequence of angular momentum conservation. We choose $n_1 = 2$ and $n_2 = 7$ in solving the above equations by the spectral method excluding $n = 1$ and $n = 0$. This trapezium truncation is illustrated in the wave–number space as shown in Fig.1. N_n^m may be rewritten in the following alternative ways in order to reduce the computing time when the expansions are being carried out algebraically.

$$N_n^m = \frac{i(-1)^m}{n(n+1)} \sum_{n''>n',|m'|\le n_1 n_2} \sum a_{n'}^{m'} a_{n''}^{m''} [n''(n''+1) - n'(n'+1)]$$

$$C(n,n',n'') \begin{bmatrix} n-1 & n' & n'' \\ 0 & 0 & 0 \end{bmatrix} \begin{bmatrix} n & n' & n'' \\ -m & m' & m'' \end{bmatrix}$$

$$= \frac{i(-1)^m}{2n(n+1)} \sum_{n'\ne n'',|m'|,|m''|\le n_1 n_2} \sum a_{n'}^{m'} a_{n''}^{m''} [n''(n''+1) - n'(n'+1)]$$

$$C(n,n',n'') \begin{bmatrix} n-1 & n' & n'' \\ 0 & 0 & 0 \end{bmatrix} \begin{bmatrix} n & n' & n'' \\ -m & m' & m'' \end{bmatrix} .$$

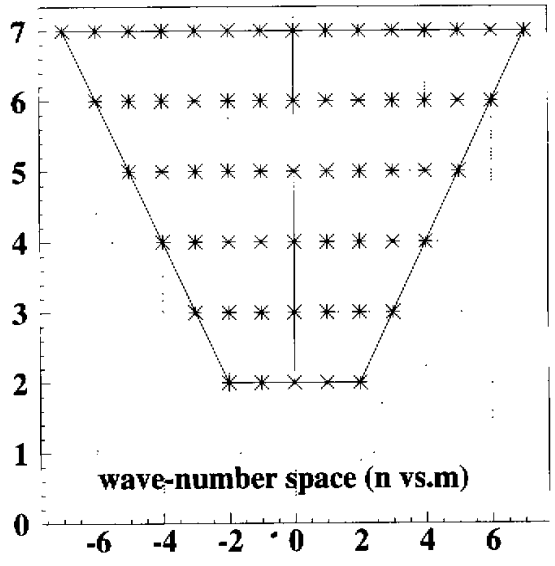

Fig. 1. The illustration of the truncated system in wave–number space ($n \sim m$). Energy and enstrophy distributions are symmetric about the central line $m = 0$.

For the sake of simplicity in calculation, some symmetries are assumed for this inviscid system. We suppose

$$a_n^m \begin{cases} i\lambda_n^m & \text{if } m \text{ is an even integer} \\ \lambda_n^m & \text{if } m \text{ is an odd integer} . \end{cases}$$

Here λ_n^m is real for every possible n and m. Therefore one has $a_n^{-m} = -a_n^m$ and $a_n^0 \equiv 0$. The symmetric distributions of energy and enstrophy about the axis $m=0$ are quite obvious due to the fact that $|a_n^m|^2 = |a_n^{-m}|^2$, which is why we consider the portion $m>0$ only. Consequently, in this system, there are 27 independent modes (a_n^m, with $n=2\cdots 7$, $m=1\cdots n$), which occupy 1672 lines if they are put together into standard double precision Fortran expressions.

III. THE EXPECTED ENERGY SPECTRUM

The way that the truncated inviscid Navier–Stokes (Euler) equations in Fourier transform space are analysed by equilibrium statistal mechanics has proved successful in providing some insight into the dynamic processes of two–dimensional turbulence (Kraichnan, 1967, 1975; Seyler et al., 1975 and Frederiksen and Sawford, 1980). Most people prefer macrocanonical to microcanonical ensembles, because the calculation in the former is much easier. Although the macrocanonical ensemble is only exact for an infinite number of degrees of freedom, it is often a good approximation for finite truncations as well. On the other hand, the microcanonical ensemble is exact for an ergodic system with a finite number of degrees of freedom. By computing the time–averaged energies and time correlations of individual modes, Kells and Orszag (1978) numerically analysed several low–order models of the inviscid two–dimensional Navier–Stokes equations and offered strong evidence in favor of a statistical description for two–dimensional isotropically truncated Navier–Stokes flows, provided that the initial conditions are arbitrary and the truncation wavenumber is at least $\geqslant\sqrt{5}$.

Frederiksen and Sawford (1980) obtained the average values of the energy and the enstrophy by means of the macrocanonical ensemble that is defined by the probability distribution. The real and imaginary parts of a_n^m are independent coordinates in the generalized phase space (Lee, 1952). The probability density in this generalized phase space is defined by

$$\begin{aligned} P(\cdots, a_n^m, \cdots) &= c\exp(-\alpha_1 E - \beta_1 \Omega) \\ &= c\exp[-\frac{1}{2}\sum_{n,m}((\alpha_1 n(n+1) + \beta_1 n^2(n+1)^2)|a_n^m|^2)], \end{aligned} \tag{10}$$

where c is a normalization parameter which is chosen so that

$$\int \cdots da_n^m \cdots P = 1. \tag{11}$$

In fact, (10), which is a thermal equilibrium ensemble, generalizes the canonical distribution of ordinary Hamiltonian mechanics. According to the canonical ensemble theory, α_1 plays the role of inverse temperature associated with the energy.① Similarly β_1 plays the role of inverse temperature corresponding to the enstrophy. Hence the expectation value of any

① Here we identify α_1 with $1/kT_E$, where k is Boltzmann's constant and T_E is temperature associated with energy.

function $f(\cdots,a_n^m,\cdots)$ is given by

$$<f> = \int P(\cdots,a_n^m,\cdots)f(\cdots,a_n^m,\cdots)\cdots da_n^m\cdots$$

The angular bracket $<\ >$ means an expectation value computed with the canonical distribution. From the energy and enstrophy expressions (7) and (8), their two–dimensional spectra are the following

$$E_n^m = \frac{1}{2}n(n+1)\left|a_n^m\right|^2,$$

$$\Omega_n^m = \frac{1}{2}n^2(n+1)^2\left|a_n^m\right|^2.$$

After considering the symmetry we have chosen in this system, one has

$$<E_n^m> = \frac{1/2}{\alpha_1+\beta_1 n(n+1)} = \frac{1}{\alpha+\beta n(n+1)}, \tag{12}$$

$$<\Omega_n^m> = \frac{(1/2)n(n+1)}{\alpha_1+\beta_1 n(n+1)} = \frac{n(n+1)}{\alpha+\beta n(n+1)}. \tag{13}$$

Here $\alpha = 2\alpha_1$ and $\beta = 2\beta_1$ are introduced for calculation convenience. We are interested in the energy distributions over n and m.

$$E(n) = \sum_{m>0} E_n^m = \frac{n}{\alpha+\beta n(n+1)} \tag{14}$$

and

$$e(m) = \sum_n E_n^m.$$

For our truncated system,

$$e(1) = e(2) = \sum_{n=2}^{7}\frac{1}{\alpha+\beta n(n+1)}, \tag{15}$$

and if $m\neq 1,2$

$$e(m) = \sum_{n=m}^{7}\frac{1}{\alpha+\beta n(n+1)}. \tag{16}$$

In Section 4, we will numerically solve (9) for a time interval which is long enough for the energy distributions over n and m become time independent. The results will be compared to the theoretical predictions from the above energy spectra. (It must be noticed that only the portion of $m>0$ is considered in all the energy formulae and numerical experiments).

Theoretically either α or β might be negative provided that $(\alpha+\beta n(n+1))>0$. Kraichnan's three equilibrum regimes, which are distinguished by the signs of α and β in a cyclic box, still exist in the present geometry (see Kraichnan, 1975 and Kraichnan et al., 1980 for details). The boundaries of the three regimes are determined by the parameter $n_c^2 \equiv \Omega/E$. The appropriate values of α and β are determined from the numerical solution of the relations

$$E = \sum_{n=n_1}^{n_2}\frac{n}{\alpha+\beta n(n+1)}, \tag{17}$$

$$\Omega = \sum_{n=n_1}^{n_2} \frac{n^2(n+1)}{\alpha + \beta n(n+1)}. \tag{18}$$

Subsequently one will see that

$$n_1(n_1+1) \leqslant n_c^2 \leqslant n_2(n_2+1).$$

The "=" sign holds only in the case of $n_1 = n_2$.

If $\alpha = 0$, we have

$$\begin{aligned} n_\alpha{}^2 = \Omega / E &= \frac{\sum_{n=n_1}^{n_2} n}{\sum_{n=n_1}^{n_2} 1/(n+1)} \\ &= \frac{(1/2)(n_2+n_1)(n_2-n_1+1)}{\Psi(n_2+2) - \Psi(n_1+1)}, \end{aligned} \tag{19}$$

where $\Psi(x)$ is the digamma function which is the logarithmic derivative of the gamma function given by $\Psi(x) \equiv \frac{d\ln\Gamma(x)}{dx}$.

If $\beta = 0$, then

$$\begin{aligned} n_\beta{}^2 = \Omega / E &= \frac{\sum_{n=n_1}^{n_2} n^2(n+1)}{\sum_{n=n_1}^{n_2} n} \\ &= (3n_1{}^3 + n_1{}^2 + 3n_1{}^2 n_2 - 2n_1 + 4n_1 n_2 + 3n_1 n_2{}^2 \\ &\quad + 3n_2{}^3 + 7n_2{}^2 + 2n_2)/(6(n_1+n_2)). \end{aligned} \tag{20}$$

Thus one can prove that $n_2(n_2+1) > n_\beta{}^2, n_\alpha{}^2 > n_1(n_1+1)$ and the three different regimes are

(I) $n_1(n_1+1) < n_c{}^2 < n_\alpha{}^2, \quad \alpha < 0, \quad \beta > 0$
(II) $n_\alpha{}^2 < n_c{}^2 < n_\beta{}^2, \quad \alpha > 0, \quad \beta > 0$
(III) $n_\beta{}^2 < n_c{}^2 < n_2(n_2+1), \quad \alpha > 0, \quad \beta < 0$

In analysing the two-dimensional turbulence in Cartesian geometry, Fox and Orszag (1973) pointed out that there is no discontinuity of any sort in crossing the boundary between the regimes. In no circumstances is there a sharp phase transition between these three regimes. The second regime is bounded by the energy-equipartition state $\beta = 0, n_c = n_\beta$ and the enstrophy equipartition state $\alpha = 0, n_c = n_\alpha$. Here the energy and enstrophy equipartitions mean the distributions over just the total wavenumber n. If $\beta = 0, E(n) \propto n$, i.e. energy equipartition; if $\alpha = 0, \Omega(n) \propto n$, i.e. enstrophy equipartition. This may be the evidence that the total wavenumber n plays a similar role to that of the wavenumber k in Cartesian geometry, as argued by Tang and Orszag (1978). Either the energy or the enstrophy equipartition state ($\alpha = 0$ or $\beta = 0$, infinite temperature!) corresponds to finite energy and enstrophy. For instance, decrease of α corresponds to increase of energy and this increase is smooth as α passes from positive to negative values. The negative temperature states may be thought of as being at temperatures higher than infinity (Kraichnan et al., 1980).

In the limits of $n_c \to \sqrt{n_1(n_1+1)}$ and $n_c \to \sqrt{n_2(n_2+1)}$, the fractions of the total energy contained in these two extreme cases approach unity. These phenomena are analogous to those in a cyclic box (Kraichnan, 1975 and Kraichnan et al., 1980). They suggested that the

condensation of the kinetic energy into n_1 corresponds to the Einstein–Bose condensation of particles into the ground state in a two–dimensional free–bose gas in finite size. However, some important differences between the 2–dimensional inviscid Navier–Stokes fluid and two–dimensional free–boson gas were also pointed out. The three regimes in our system ($n_1 = 2$ and $n_2 = 7$) are decided by the values of $n_c{}^2$. The minimum and maximum values of $n_c{}^2$ are 6.0, 56.0 respectively, and $n_\alpha{}^2 \approx 22.1701$, $n_\beta{}^2 \approx 34.1481$. In order to test the energy distributions in the different regimes, we intentionally choose the initial locations to achieve the desired values of $n_c{}^2$ as described in the next section.

IV. NUMERICAL EXPERIMENTS

The purpose of this section is to present the results from numerical treatment of the truncated inviscid equations (9) when the average energy distributions of the system become time independent after long enough time integrations. The differences between the experimental results and the expected ones described in the above section can be displayed in the three equilibrium regimes. The method we use to solve the spectral equations (9) along with the nonlinear expression (6) is the fourth–order Runge–Kutta in double precision Fortran. The time step for all computation in this paper is 1 / 1000. Two of the four cases for which we have solved are in the regime I. The other two correspond to the regimes *II* and *III*. The initial locations of nonzero a_n^m are chosen to achieve the desired values of $n_c{}^2$, which are shown in Table 1. Each initial loading consists of $a_n^m = 0$, except for a few values of n and m. The energy and enstrophy become transferred to both larger and smaller scales to arrive at equilibrium distributions by the nonlinear action. The accuracy in our computation is believed to be quite high, although the expressions for the nonlinear terms (6) are extremely long. The conservation of E and Ω is our principal accuracy check and this is displayed in Table 2. The error values in this table are the instantaneous ones corresponding to the last step of each period.

Table 1. Computation Parameters

Run	Regime	E	Ω	$n_c{}^2$	α	β
A	I	0.0205	0.2318	11.2844	−1201.6024	222.5554
B	I	1.3849	16.7045	12.0612	−15.1531	2.8728
C	*III*	20.5887	932.9273	45.3125	4.3727	−0.0675
D	*II*	0.5918	13.4272	22.6884	1.3868	1.9497

Table 2. Test of Computation Accuracy

Run	$10^{15} \times \lvert\Delta E\rvert / E$			$10^{15} \times \lvert\Delta\Omega\rvert / \Omega$		
	5500	10500	95500	5500	10500	95500
A	0.717	1.456	1.288	0.688	1.422	1.242
B	9.840	1.303	97.036	5.875	30.201	210.793
C	441.506	993.492	24098.694	2214.507	2521.062	23796.947
D	1.524	0.117	1.102	0.695	1.935	5.672

Figures 2a, 3a, 4a, 5a show the energy spectra as a function of total wave–number n for runs A, B,C, and D. In the panels labelled (1), the initial energy spectra $E(n)$ are plotted against n. For the runs A,B,C, the initial points in the phase space are randomly chosen apart from fixing the desired values of n_c^2. In regime *II*, we have chosen more nonzero modes than the other regimes and let the spectrum be much closer to the expected as shown in the Run D(1) in Figure 5a. The panels labelled (2), (3) and (4) represent the time–averaged spectra over 500 time steps in three different periods (5000–5500, 10000–10500 and 95000–95500) respectively for the four runs together with the theoretical predictions as shown by dashed curves. For runs A,B, and C, the computational results agree with the theoretical ones very well. The time averaged spectra show a systematic tendency toward equilibium after some relaxation time. Each numerical result at the equilibrium is put into a spectrum form of $E(n)=an^b$ with real a and b by finding least–square fits. All the simulated formulas for the three periods are shown in Table 3. They are also displayed by the dotted curves in these figures. There are negative values of α in both runs A and B, but run A has larger absolute value of $\alpha(\approx -1201.6024)$ and closer value of $n_c^2(\approx 11.2844)$ to the lower boundary $(=6.0)$ than run B. As a result, it has steeper distributions ($n^{-5.352}$, $n^{-3.638}$ and $n^{-3.176}$ in the three periods). The lowest mode $(n=2)$ has 53.448% of the total energy in the last period of run A.

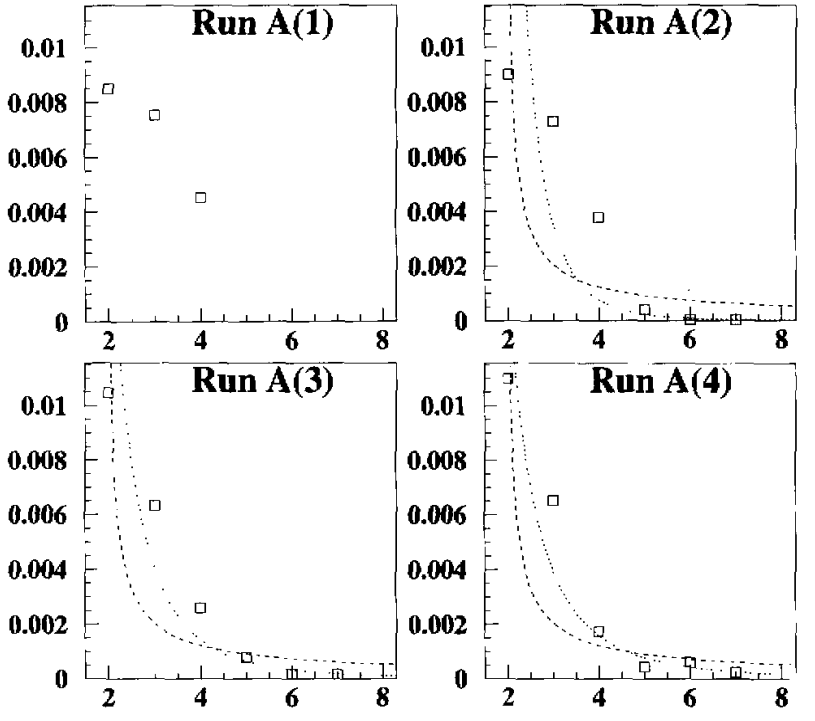

Fig.2a. Energy spectra over n for run A. (1) initial one; (2) a time average over 500 time steps (5000–5500); (3) a time average over steps (10000–10500); (4) a time average over the last 500 time steps (95000–95500). The square symbols represent the experimental distributions. The dashed curves are the theoretical prediction, Eq. (14). The dotted ones are the simulated energy formulas from the numerical results.

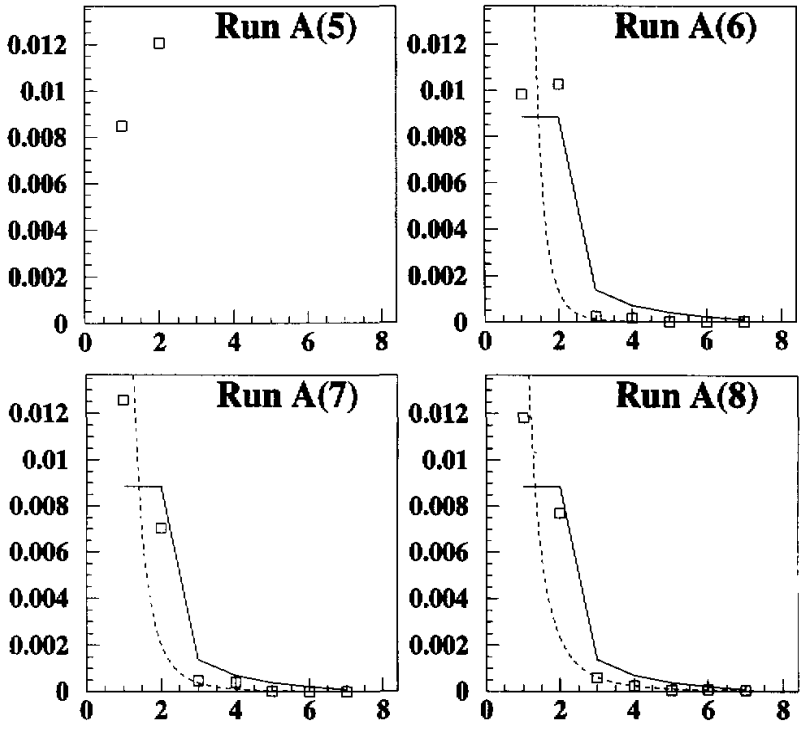

Fig. 2b. Energy spectra over m for run A. (5) initial one; (6) a time average over 500 time steps (5000–5500); (7) a time average over steps (10000–10500); (8) a time average over the last 500 time steps (95000–95500) . The square symbols represent the experimental distributions. The solid curves are the theoretical prediction, Eqs. (15) (16). The dashed ones are the simulated energy formulas from the numerical results.

Table 3. Simulated Energy Formulae $E(n)$, $e(m)$

Steps	Run A	Run B	Run C
5000–	$1.265n^{-5.352}$	$5.648n^{-2.777}$	$0.019n^{3.109}$
5500	$0.087m^{-6.012}$	$1.882m^{-3.078}$	$9.048m^{-1.464}$
10000–	$0.224n^{-3.638}$	$1.288n^{-1.957}$	$0.026n^{2.904}$
10500	$0.038m^{-4.183}$	$0.683m^{-2.524}$	$4.062m^{-0.366}$
95000–	$0.130n^{-3.176}$	$4.544n^{-2.647}$	$0.063n^{2.371}$
95500	$0.022m^{-3.234}$	$1.047m^{-2.623}$	$3.871m^{-0.502}$

In run C, the value of β is negative so that the spectra appear in an opposite way. The powers in the simulated formulas vary from 3.109 to 2.371 in the last period of the run with (63.439%) of the total energy on the highest mode ($n=7$), via 2.904 in the middle period of the run. Run D belongs to the second regime, which is the most ordinary case with both positive values of α and β. However, the experimental and expected results are far apart, although an initial spectrum similar to the expected one was chosen. It is obvious that the longer it

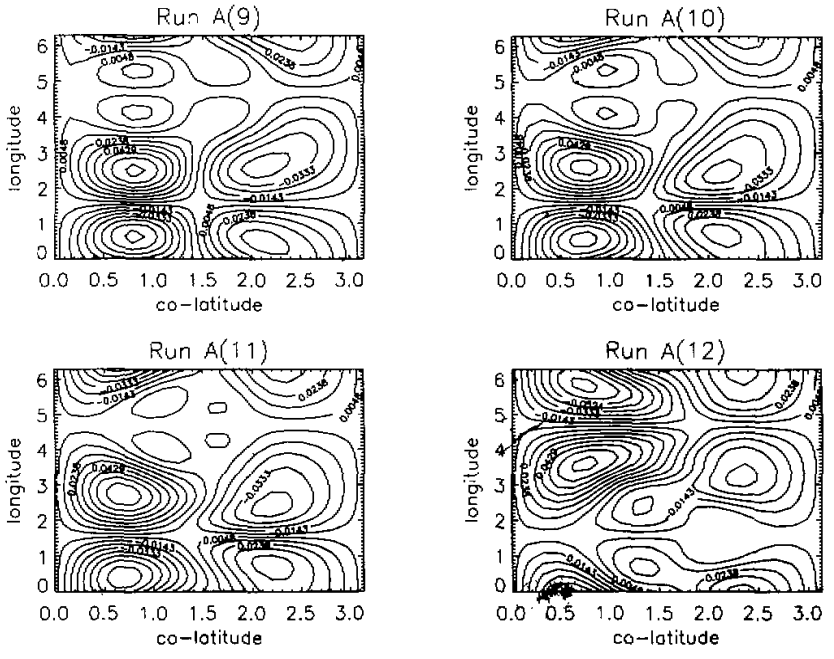

Fig. 2c. Contours of constant $\psi(\theta,\varphi,t)$ with $\theta(0 \leqslant \theta \leqslant \pi)$ in the horizontal direction and $\varphi(0 \leqslant \varphi \leqslant 2\pi)$ in the vertical direction for run A. The times for the four instantaneous sets of streamlines are at step 0, step 5500, step 10500 and the last step of the run (from left to right).

runs, the further away from prediction it becomes. In the final period, the spectrum is so irregular and chaotic that we can't put it into any known form. It is quite uncertain whether the system in this regime will reach an eventual equilibrium state.

Figures 2b, 3b, 4b and 5b display the energy spectra as a function of zonal wavenumber m for runs A,B,C, and D. The panels labelled (5), (6), (7) and (8) show the initial loadings and those in other three periods described above for each run. The theoretical points from equations (15) and (16) are connected by the solid straight lines in the figures. The values of $m=1$ and 2 are equal due to the man–made truncation in this system. If we fit these distributions into the same form as those for n, i.e. $e(m)=cm^d$ with real c and d, then, the powers vary from −6.011, −4.183 to −3.234 in the last period for run A, which are steeper than those in run B as shown in Table 3. The fits for run C are little reluctant somehow compared with the situations in runs A and B due to the fact that the distributions in run C are not so regular as those in runs A and B. The spectra in run D (i.e. in regime *II*) are quite irregular after some time. The longer it evolves, the more irregular it becomes.

In the figures 2c, 3c, 4c and 5c the contours of stream function $\psi(\theta,\varphi,t)$ in physical space (θ,φ), which is defined by (3), are plotted at the beginning (first step in each run) and the end of each period for each run. The panels labelled (9), (10), (11) and (12) show the streamlines at start, step 5500, step 10500 and step 95500 respectively in each run. The most impressive feature in these figures, which is different from that in cyclic boundary observed by Seyler et al. (1975), perhaps is that the vortex structures in the equilibrium state (say the final period)

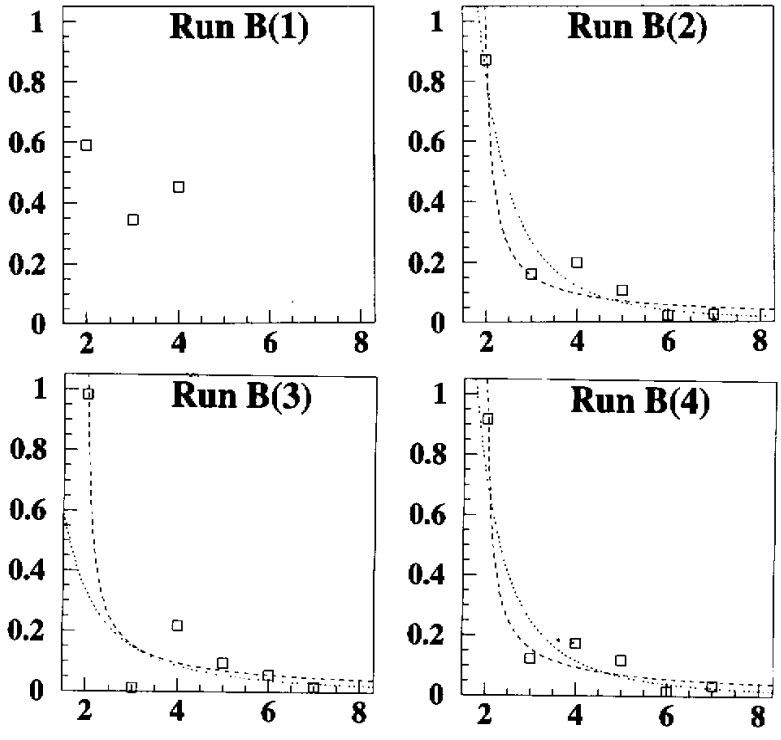

Fig. 3a. Energy spectra over n for run B. (1) initial one; (2) a time average over 500 time steps (5000–5500); (3) a time average over steps (10000–10500); (4) a time average over the last 500 time steps (95000–95500). The square symbols represent the experimental distributions. The dashed curves are the theoretical prediction, Eq. (14). The dotted ones are the simulated energy formulas from the numerical results.

in run A with $\alpha=-1201.6024$ are not obviously larger than those in run B with $\alpha=-15.1531$. The vortices in run A are larger in the longitudinal direction only, but smaller in latitudinal direction than those in run B.

Run C has the smallest vortices at each instant, so that it has the largest number of vortices all the time. Run D is second to run C in this sense. Both runs C and D have smaller vortices than those in runs A and B. This phenomenon may imply that the flow in the equilibrium state regime *II*, especially regime *III*, has weaker interaction between different parts than that in regime I due to the larger values of n_c^2 (see Table 1). A conclusion that different parts of the flow with higher value of n_c^2 have weaker interaction and behave in more relative isolation needs to be analysed further.

V. ENTROPY EVOLUTIONS

We next try to analyze the ergodicity of our system which plays an important role in our numerical simulations. According to Betchov (1964), the entropy may be defined as

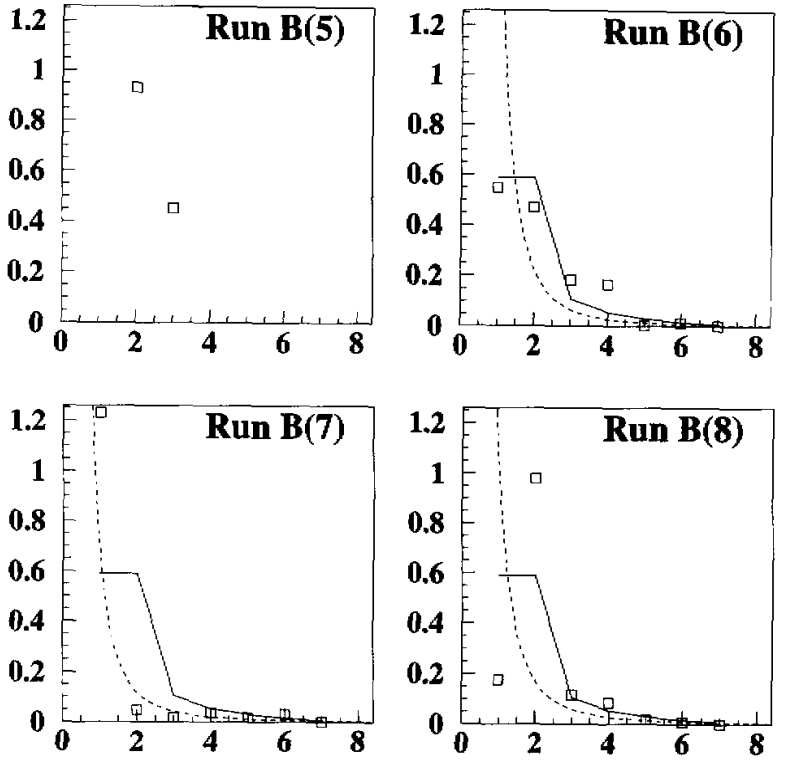

Fig. 3b. Energy spectra over m for run B. (5) initial one; (6) a time average over 500 time steps (5000–5500); (7) a time average over steps (10000–10500); (8) a time average over the last 500 time steps (95000–95500). The square symbols represent the experimental distributions. The solid curves are the theoretical prediction, Eqs. (15) (16). The dashed ones are the simulated energy formulas from the numerical results.

$$S(t) = \sum_{n,m} \ln E_n^m(t) = \sum_{n,m} \ln[n(n+1)\left|a_n^m(t)\right|^2 / 2]. \tag{21}$$

Betchov (1964) argued that this quantity is a measure of the information necessary to specify the turbulent motion of a fluid with energy spectrum E_n^m. A more general analytical study of this quantity and H theorem for inviscid flow can be found in Carnevales et al. (1981). The theoretical prediction for this quantity was shown to be consistent with the numerical simulations of a two–dimensional flow with a circular truncation by Carnevale (1982). An analogous calculation will be carried out for our system. It is necessary to assume $\left|a_n^m\right| > 0$ to calculate dS/dt from equation (21), which implies that all modes have non–zero energy. Thus one can obtain

$$\frac{dS}{dt} = 2\sum_{n,m} Re\left(\frac{N_n^m}{a_n^m}\right) - 2\nu\sum_{n,m} n(n+1). \tag{22}$$

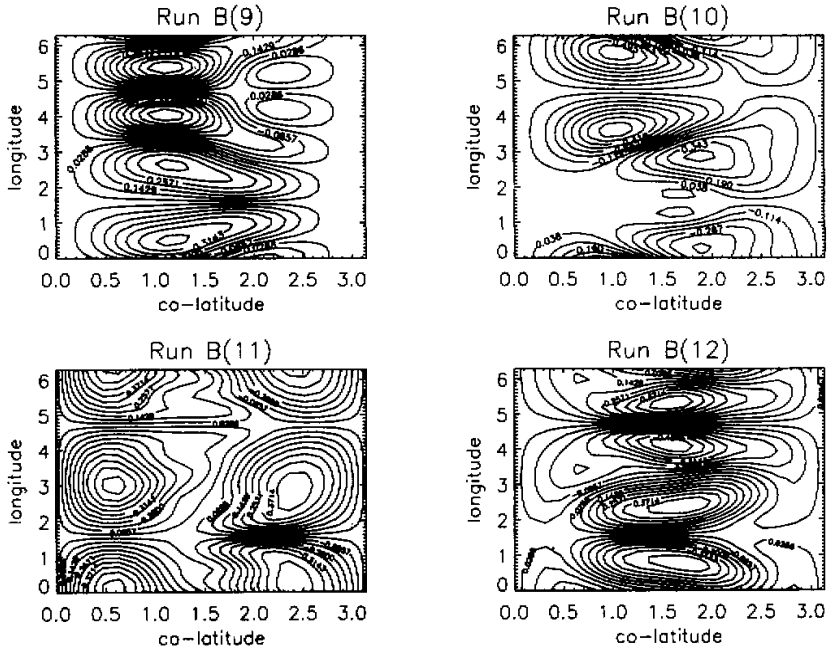

Fig. 3c. Contours of constant $\psi(\theta,\varphi,t)$ with $\theta(0 \leqslant \theta \leqslant \pi)$ in the horizontal direction and $\varphi(0 \leqslant \varphi \leqslant 2\pi)$ in the vertical direction for run B. The times for the four instantaneous sets of streamlines are step 0, step 5500, step 10500 and the last step of the run (from left to right).

Any attempts at an analytical study of the above entropy equation have proved difficult due to the complexity of the nonlinear expression N_n^m. From the results of above sections, the expected energy spectra in runs A and B are more consistent with the numerical ones than those in run C. Run D was supposed to be non-ergodic anyway. We calculate the entropy in each of the first three runs. Figures 6a, 6b and 6c show the entropy evolutions with time of runs A, B and C respectively. The computation for run A is carried out until $t=95.5$ (i.e. the time-step 95500) and $t=10$ for runs B and C. The value of equilibrium entropy S_{eq} in each run is indicated by a dash-dotted line, and

$$S_{eq} \sum_{n,m} \ln < E_n^m(t) > = -\sum_n n \ln[\alpha + \beta n(n+1)]. \tag{23}$$

According to (10), the equilibrium expectation value of entropy ($< S(t) >$) shown by the dashed line in each run is given by

$$< S(t) > = \int P(\cdots, a_n^m, \cdots) S(t) (\cdots, a_n^m, \cdots) \cdots da_n^m \cdots \tag{24}$$

The value of the entropy near equilibrium after some time should agree well with the theoretical $< S >$. Considering the symmetry we have chosen in this system, $< S >$ can be calculated directly as

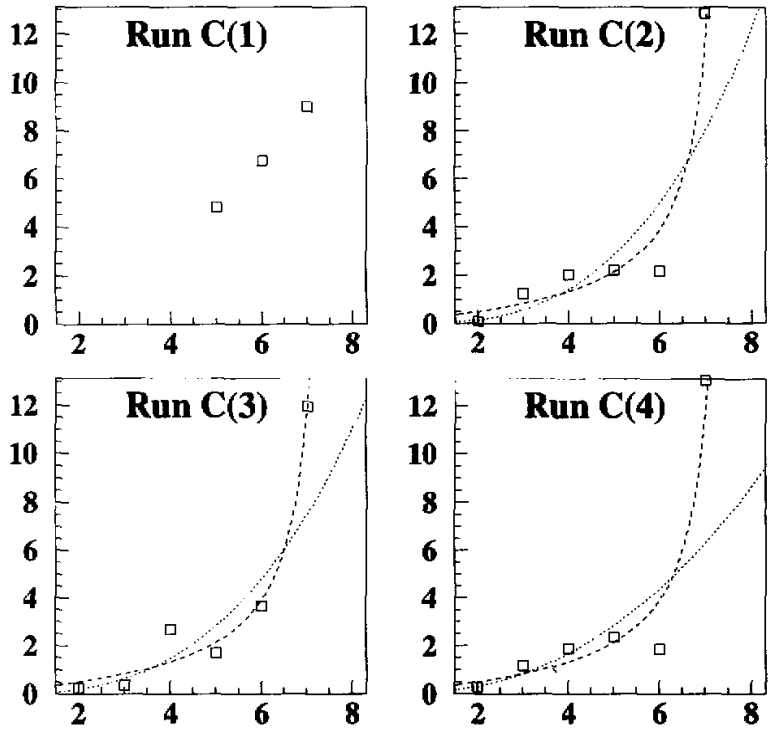

Fig. 4a. Energy spectra over n for run C. (1) initial one; (2) a time average over 500 time steps (5000–5500); (3) a time average over steps (10000–10500); (4) a time average over the last 500 time steps (95000–95500). The square symbols represent the experimental distributions. The dashed curves are the theoretical prediction, Eq. (14). The dotted ones are the simulated energy formulas from the numerical results.

$$< S > = S_{eq} - N(\gamma + \ln 2), \tag{25}$$

where N is the total number of independent modes in this system, and γ is the standard Euler's constant.①The expression for $<S>$ for a more general choice of coefficients can be found in the Appendix.

Theoretically, there are some slight fluctuations in canonical statistical mechanics due to the interaction with the surrounding "heat bath". The phase point stays almost exactly on the multiple invariant subspace which is the intersection of the surfaces corresponding to the integral invariants (the energy and enstrophy in this case) of the system for a canonical ensemble. The predicted standard deviation can also be computed on the basis of the canonical distribution (10)

$$\Delta S \equiv \sqrt{< (S - < S >)^2 >} = \sqrt{< S^2 > - < S >^2}$$
$$= \sqrt{N(\pi^2 / 2 - 2\gamma \ln 2)} = 10.5657. \tag{26}$$

①i.e. $\gamma = \lim_{m \to \infty} [\sum_{k=1}^{m} (\frac{1}{k}) - \ln m] \approx 0.57722$.

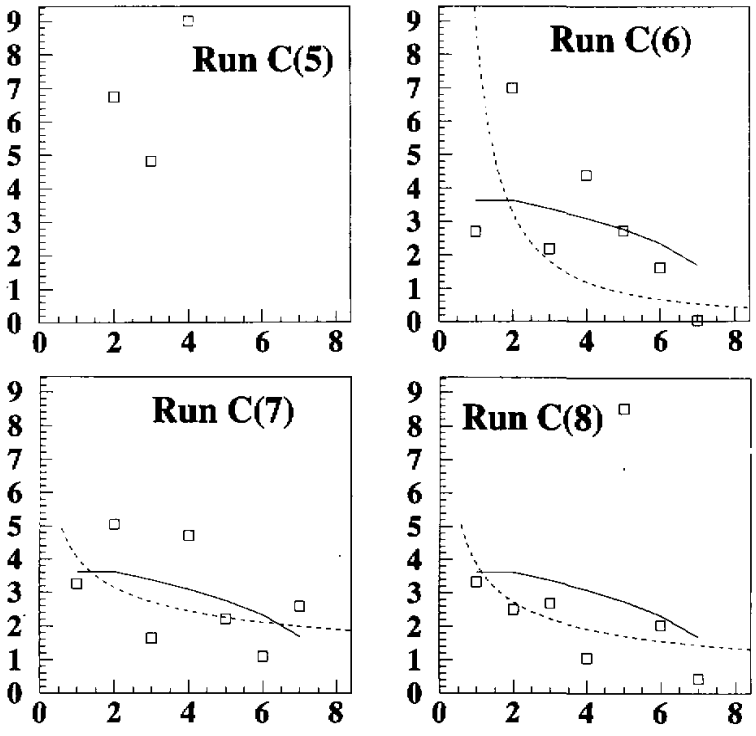

Fig. 4b. Energy spectra over m for run C. (5) initial one; (6) a time average over 500 time steps (5000–5500); (7) a time average over steps (10000–10500); (8) a time average over the last 500 time steps (95000–95500). The square symbols represent the experimental distributions. The solid curves are the theoretical prediction, Eqs. (15) (16). The dashed ones are the simulated energy formulas from the numerical results.

The predicted deviations $< S > \pm \Delta S$ about $< S >$ are indicated by two dotted lines shown in Figs. 6a, 6b and 6c. The above results are also shown in Table 4.

Table 4. Entropy and Entropy Fluctuations

Run	n_c^2	α	β	S_{eq}	$< S > \pm \Delta S$
A(I)	11.2844	−1201.6024	222.5554	−226.3891	−260.6889 ± 10.5657
B(I)	12.0612	−15.1531	2.8728	−109.4713	−143.7711 ± 10.5657
C(*III*)	45.3125	4.3727	−0.0675	−14.1800	−48.4800 ± 10.5657
D(*II*)	22.6884	1.3868	1.9497		

The entropy in each of the three runs increases rapidly and smoothly in the early period, which is exactly as predicted theoretically. Runs B and C with smaller absolute values of $<S>$ approach equilibrium sooner than run A. Actually, run A whose energy spectra were more consistent with the expected ones in our previous results takes a longer time to arrive the

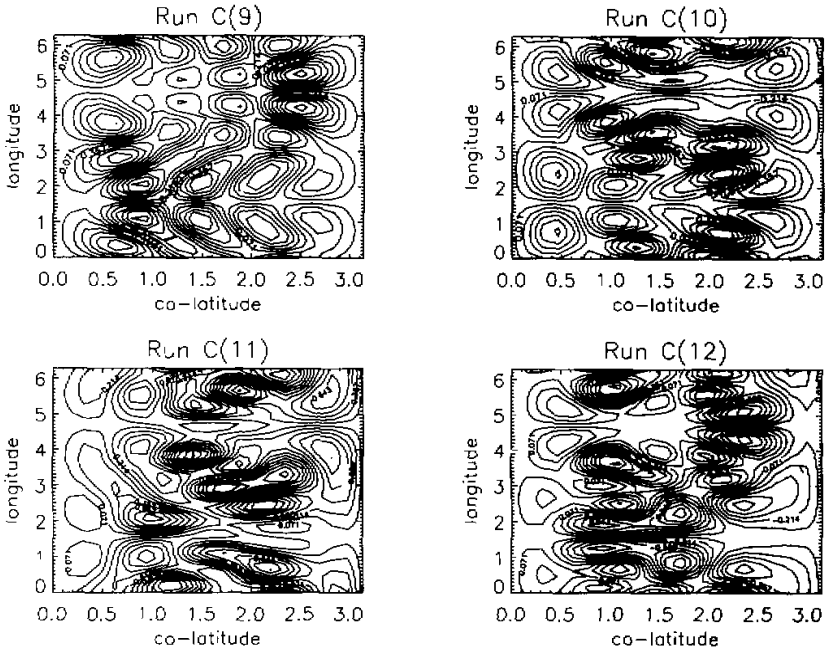

Fig. 4c. Contours of constant $\psi(\theta,\varphi,t)$ with $\theta(0 \leqslant \theta \leqslant \pi)$ in the horizontal direction and $\varphi(0 \leqslant \varphi \leqslant 2\pi)$ in the vertical direction for run C. The times for the four instantaneous sets of streamlines are at step 0, step 5500, step 10500 and the last step of the run (from left to right).

equilibrium state. From our computation, runs A,B,C did not enter their equilibrium regions until about $t = 11.333$, 1.200 and 0.567 respectively. However, run A has the smallest value of relative fluctuation once it has achieved equilibrium. In conclusion, the entropy in each of the three runs evolves reasonably well within the expected range.

To test the entropy in a dissipative system, we chose run A as an example with 0.001 and 0.002 as values for the viscosity. The results are also displayed in Figure 6a. Intuitively, the effect of viscosity resists the motions of fluid flows and consequently increases the order of the system and also our information about the state of the system. Therefore, the entropy of the system should decrease when viscosity becomes dominant. More further, the entropy decay rates should be proportional to the values of the viscosity of the system from equation (22), once the viscosity is dominant. These conclusions have been confirmed from our numerical experiments. A certain amount of fluctuation still remains even if viscosity is dominant from Fig. 6a.

Run D is supposed to be non-ergodic from the energy spectrum simulations. The broken ergodicity of the ensemble in this run is quite obvious from the definition of entropy (21). The infinite entropy fluctuation would appear due to the existence of some zero energy modes in whole run. The non-ergodicity in this run may indicate coherent structures in the phase space. Coherent structures in the phase space result from coherent structures in the physical space according to Shebalin (1989). He also demonstrated that ideal fluid (i.e. Euler) flow in a two-dimensional periodic box is ergodic and that ideal 2-dimensional magnetohydro-

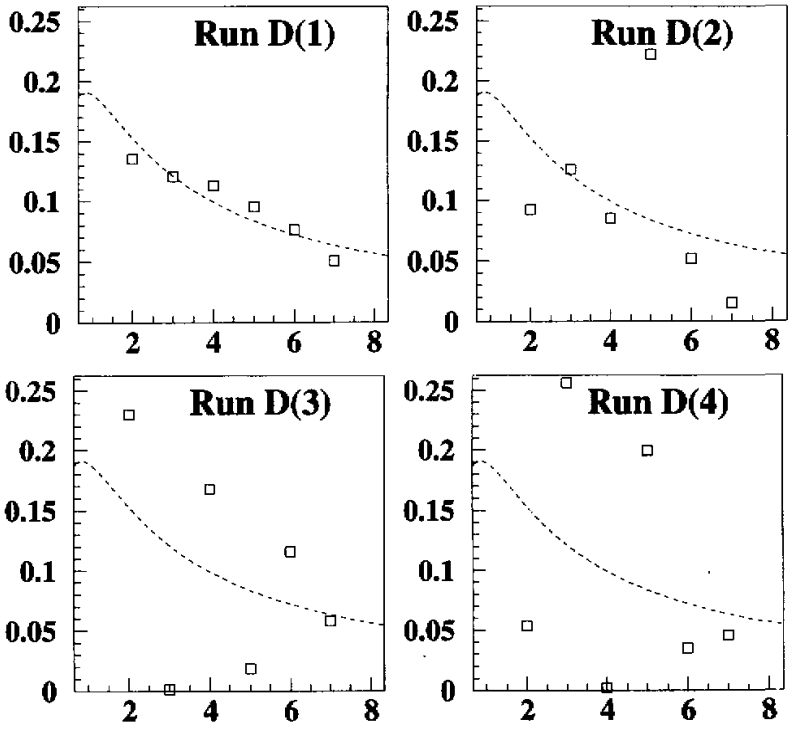

Fig. 5a. Energy spectra over n for run D. (1) initial one; (2) a time average over 500 time steps (5000–5500); (3) a time average over steps (10000–10500); (4) a time average over the last 500 time steps (95000–95500). The square symbols represent the experimental distributions. The dashed curves are the theoretical prediction, Eq. (14).

dynamical flows do not appear to be ergodic according to a number of computer simulations. From our results, the coherent structures of Euler flows in the spherical geometry still exist, but depend on the initial conditions. In this sense, 2D ideal flows on the sphere have a less pronounced tendency to be ergodic than those on planar geometry. We believe this is due to the curvature of the spherical surface that weakens the interaction between different parts of the flow, enabling these parts to behave in a more relative isolation.

VI. SOME REMARKS

It is assumed that the only constants of the system are energy and enstrophy in the present work. The absolute equilibrium treatment of the inviscid two–dimensional incompressible flows after a long enough time means eventually that the flows on the intersection of the surfaces of the two constants are mixing ①in the phase space. The unresolved problem is the possible existence of the other constants of the motion in addition to the energy and the enstrophy, particularly in run D. The non–ergodicity of run D might be caused or partly caused by those constants except for the energy and the enstrophy which are considered in

①Strictly speaking, mixing implies ergodicity, but ergodicity does not imply mixing.

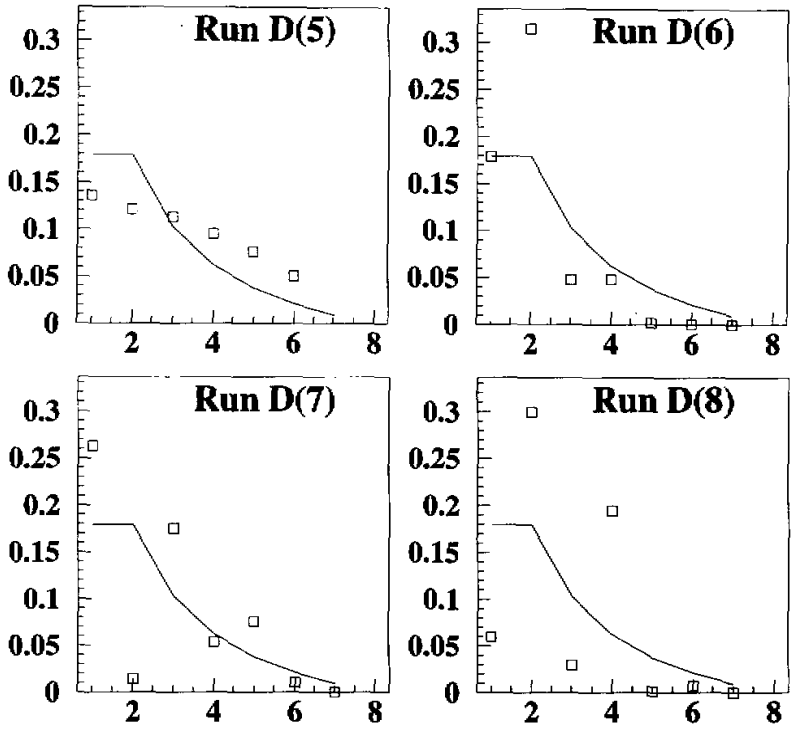

Fig. 5b. Energy spectra over m for run D. (5) initial one; (6) a time average over 500 time steps (5000–5500); (7) a time average over steps (10000–10500); (8) a time average over the last 500 time steps (95000–95500). The square symbols represent the experimental distributions. The solid curves are the theoretical prediction, Eqs. (15) (16).

our study. Owing to the complexity of the chosen system, it is not practical for us to answer it by exact analysis. The consistency of the numerical results and predicted ones in runs A, B and C does give us some confidence that the system in those regimes is ergodic or mixing. The fact that the discrepancy occurs in the most ordinary regime (with two positive temperatures) might imply that a state in regime *II* has less tendency to be ergodic or mixing, and the flows in both regimes *I* and *III* have more pronounced tendencies to achieve absolute equilibrium states. However, more numerical and technical tests are needed to arrive a definite conclusion. For instance, numerical computation could be carried out for a much longer time on a more powerful machine. The enlargement of truncation size may increase the chances of system becoming ergodic or mixing, although the minimum number of modes required to obtain ergodic or mixing behaviour is not known precisely. The microcanonical ensemble could be a good candidate for describing this system, except for the computational difficulty, since it is better for an isolated system. The time correlation function defined by Kells and Orszag (1978) could also be used to test whether the system could be ergodic or mixing in this regime. The results for the energy spectra over zonal wave–number m show that m is not in a good position as n for analysing the equilibrium two–dimensional inviscid flows, at least in the low–order models. In physical space, the vortex scales in the run with greater negative values

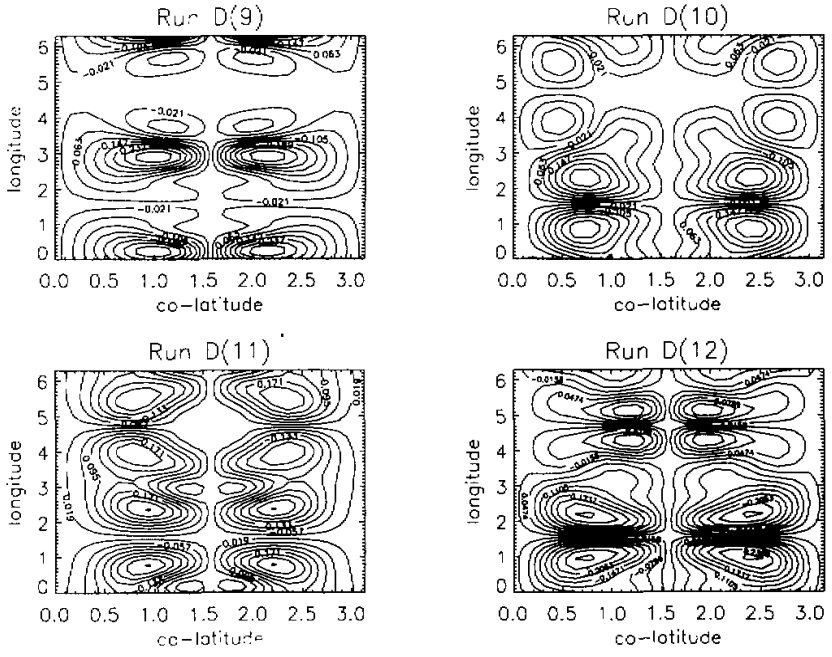

Fig. 5c. Contours of constant $\psi(\theta,\varphi,t)$ with $(0 \leqslant \theta \leqslant \pi)$ in the horizontal direction and $\varphi(0 \leqslant \varphi \leqslant 2\pi)$ in the vertical direction for run D. The times for the four instantaneous sets of streamlines are at step 0, step 5500, step 10500 and the last step of the run (from left to right).

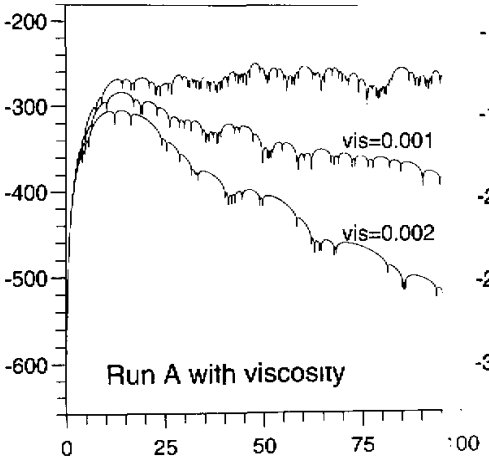

Fig. 6a. The entropy evolutions of run A with and without viscosity.

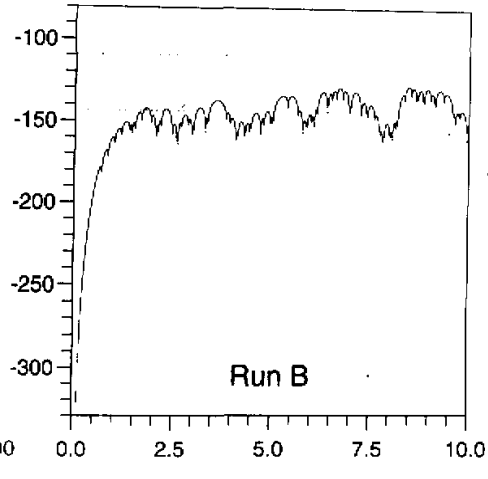

Fig. 6b. The entropy evolution of run B without viscosity.

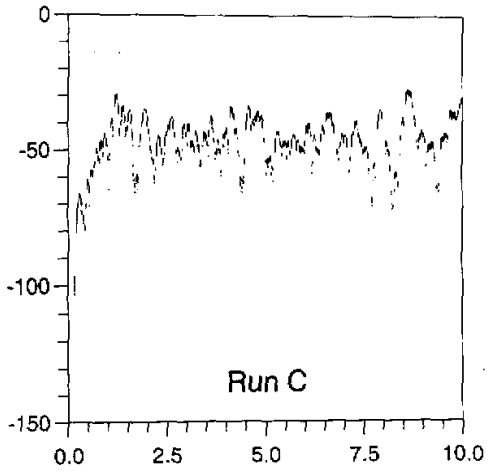

Fig. 6c. The entropy evolutions of run C without viscosity.

of α are larger in the longitudinal direction, but smaller in the latitudinal direction, than those with less negative values of α. This is not exactly similar to the situation in Cartesian geometry. A conclusion may be drawn from the contour plots of the stream function that different parts of the flow with higher value of n_c^2 have weaker interaction and behave in more relative isolation. To generalize this conclusion still needs further work.

I thank J.S. Dowker for his helpful discussion and comments during the early state of this work.

APPENDIX. CALCULATIONS OF CANONICAL FLUCTUATIONS

The generalized phase space may be defined as a Hilbert space (Lee, 1952) whose axes are the independent real and imaginary parts of the components $a_n^m (n = n_1 \cdots n_2$ and $m = -n \cdots n)$ of the steram function $\psi(\theta, \varphi, t) = \sum_{n=n_1}^{n_2} \sum_{|m| \leqslant n} a_n^m(t) Y_m^n(\theta, \varphi)$. The trajectory of phase points in this phase space is determined by the dynamical equations (5). Generally speaking, the motion of the phase points is restricted exactly (for a microcanonical ensemble) or almost exactly (for a canonical ensemble) to lie on a multiply invariant subspace with lower dimension, which is the intersection of a number of integral invariant surfaces of the system considered. The equilibrium average of entropy $<\mathbf{S}>$ defined by (24) and the standard deviation ΔS in a canonical ensemble defined by (26) depend on the symmetry one imposes on the system and choice of components a_n^m. Here we would like to discuss two different component choices. The results show that our choice of coefficients of the stream function makes a larger range of fluctuation available.

Case 1. This is the case we have considered in this paper, i.e. a_n^m is chosen as

$$a_n^m = \begin{cases} i\lambda_n^m & \text{if } m \text{ is an even integer} \\ \lambda_n^m & \text{if } m \text{ is an odd integer} . \end{cases}$$

Here λ_n^m is real for every possible n and m. From (24), one obtains

$$
\begin{aligned}
<S> &= \int\cdots\int C_n e^{-\alpha_1 E-\beta_1\Omega}\sum_{n,m}\ln[n(n+1)|a_n^m|^2/2]\cdots da_n^m\cdots \\
&= \frac{\sum_{n,m}\int_{-\infty}^{+\infty}\cdots\int_{-\infty}^{+\infty}\ln[n(n+1)\lambda_n^{m^2}/2]e^{-\alpha_1 E-\beta_1\Omega}\cdots d\lambda_n^m\cdots}{\int_{-\infty}^{+\infty}\cdots\int_{-\infty}^{+\infty}e^{-\alpha_1 E-\beta_1\Omega}\cdots d\lambda_n^m\cdots} \\
&= \sum_{n,m}\left\{\ln[\frac{1/4}{\alpha_1+\beta_1 n(n+1)}]-\gamma\right\} \\
&= S_{eq}-N(\gamma+\ln 2)\ . \qquad (27)
\end{aligned}
$$

C_n in above expression is a normalization constant, and is chosen so that

$$\int\cdots\int C_n e^{-\alpha_1 E-\beta_1\Omega}\cdots da_n^m\cdots = 1.$$

Analogous to above calculation,

$$
\begin{aligned}
<S^2> &= \int\cdots\int C_n e^{-\alpha_1 E-\beta_1\Omega}\cdots da_n^m\cdots \\
&\quad \sum_{n,m,n',m'}\ln[n(n+1)|a_n^m|^2/2]\ln[n'(n'+1)|a_{n'}^{m'}|^2/2] \\
&= \sum_{n,m}\frac{\int_{-\infty}^{+\infty}\ln^2[n(n+1)\lambda_n^{m^2}/2]e^{-\alpha_1 E_n^m-\beta_1\Omega_n^m}d\lambda_n^m}{\int_{-\infty}^{+\infty}e^{-\alpha_1 E_n^m-\beta_1\Omega_n^m}d\lambda_n^m}+ \\
&\quad \sum_{(n,m)\neq(n',m')}\left\{\int_{-\infty}^{+\infty}\int_{-\infty}^{+\infty}\ln[n(n+1)\lambda_n^{m^2}/2]\ln[n'(n'+1)\lambda_{n'}^{m'^2}/2]\right. \\
&\quad \left.\cdot e^{-\alpha_1 E_n^m-\beta_1\Omega_n^m-\alpha_1 E_{n'}^{m'}-\beta_1\Omega_{n'}^{m'}}d\lambda_n^m d\lambda_{n'}^{m'}\right\} \\
&\quad \Big/\left\{\int_{-\infty}^{+\infty}\int_{-\infty}^{+\infty}e^{-\alpha_1 E_n^m-\beta_1\Omega_n^m}\ -\ -\alpha_1 E_{n'}^{m'}-\beta_1\Omega_{n'}^{m'}d\lambda_n^m d\lambda_{n'}^{m'}\right\} \\
&= \sum_{n,m}[\ln^2\frac{1}{\alpha+\beta n(n+1)}-2(\gamma+\ln 2)\ln\frac{1}{\alpha+\beta n(n+1)}+\gamma^2 \\
&\quad +\ln^2 2+\pi^2/2]+\sum_{(n,m)\neq(n',m')}\left\{[\ln\frac{1}{\alpha+\beta n(n+1)}-\ln 2-\gamma]\right. \\
&\quad \left.\cdot[\ln\frac{1}{\alpha+\beta n'(n'+1)}-\ln 2-\gamma]\right\} \\
&= \sum_{n,m,n',m'}\left\{[\ln\frac{1}{\alpha+\beta n(n+1)}-\ln 2-\gamma][\ln\frac{1}{\alpha+\beta n'(n'+1)}\right. \\
&\quad \left.-\ln 2-\gamma]\right\}+N(\pi^2/2-2\gamma\ln 2)\ . \qquad (28)
\end{aligned}
$$

From the expressions of $<S>$ and $<S^2>$, one can obtain

$$\Delta S_1 = \sqrt{< S^2 > - < S >^2} = \sqrt{N(\pi^2/2 - 2\gamma\ln 2)}. \tag{29}$$

Case 2. If the a_n^m are assumed taken generally complex

$$a_n^m = x_n^m + iy_n^m,$$

where x_n^m and y_n^m are real, then the dimension of phase space is twice of that of case 1,

$$\begin{aligned} < S > &= \int\cdots\int C_n e^{-\alpha_1 E - \beta_1 \Omega} \sum_{n,m} \ln[n(n+1)|a_n^m|^2/2] \cdots da_n^m \cdots \\ &= \sum_{n,m} \left\{ \int_{-\infty}^{+\infty}\int_{-\infty}^{+\infty} \ln[n(n+1)(x_n^{m^2} + y_n^{m^2})/2] e^{-\alpha_1 E_n^m - \beta_1 \Omega_n^m} \right. \\ &\quad \left. \cdot dx_n^m dy_n^m \right\} \Big/ \left\{ \int_{-\infty}^{+\infty}\int_{-\infty}^{+\infty} e^{-\alpha_1 E_n^m - \beta_1 \Omega_n^m} dx_n^m dy_n^m \right\} \\ &= \sum_{n,m} \frac{1}{\alpha_1 + \beta_1 n(n+1)} - N\gamma. \end{aligned} \tag{30}$$

Again the average of entropy square $< S^2 >$ can be calculated,

$$\begin{aligned} < S^2 > &= \sum_{n,m} \left\{ \int_{-\infty}^{+\infty}\int_{-\infty}^{+\infty} \ln^2[n(n+1)(x_n^{m^2} + y_n^{m^2})/2] e^{-\alpha_1 E_n^m - \beta_1 \Omega_n^m} \right. \\ &\quad \left. \cdot dx_n^m dy_n^m \right\} \Big/ \left\{ \int_{-\infty}^{+\infty}\int_{-\infty}^{+\infty} e^{-\alpha_1 E_n^m - \beta_1 \Omega_n^m} dx_n^m dy_n^m \right\} + \\ &\quad \sum_{(n,m)\neq(n',m')} \left\{ \int_{-\infty}^{+\infty}\int_{-\infty}^{+\infty}\int_{-\infty}^{+\infty}\int_{-\infty}^{+\infty} \ln[n(n+1)(x_n^{m^2} + y_n^{m^2})/2] \right. \\ &\quad \cdot \ln[n'(n'+1)(x_{n'}^{m'^2} + y_{n'}^{m'^2})/2] e^{-\alpha_1 E_n^m - \beta_1 \Omega_n^m - \alpha_1 E_{n'}^{m'} - \beta_1 \Omega_{n'}^{m'}} \\ &\quad \left. \cdot dx_n^m dy_n^m dx_{n'}^{m'} dy_{n'}^{m'} \right\} \Big/ \left\{ \int_{-\infty}^{+\infty}\int_{-\infty}^{+\infty}\int_{-\infty}^{+\infty}\int_{-\infty}^{+\infty} \right. \\ &\quad \left. \cdot e^{-\alpha_1 E_n^m - \beta_1 \Omega_n^m - \alpha_1 E_{n'}^{m'} - \beta_1 \Omega_{n'}^{m'}} dx_n^m dy_n^m dx_{n'}^{m'} dy_{n'}^{m'} \right\} \\ &= \sum_{n,m} \left\{ [\ln \frac{1}{\alpha_1 + \beta_1 n(n+1)} - \gamma]^2 + \pi^2/6 \right\} + \\ &\quad \sum_{(n,m)\neq(n',m')} \left\{ [\ln \frac{1}{\alpha_1 + \beta_1 n(n+1)} - \gamma][\ln \frac{1}{\alpha_1 + \beta_1 n'(n'+1)} - \gamma] \right\} \\ &= \sum_{n,m,n',m'} \left\{ [\ln \frac{1}{\alpha_1 + \beta_1 n(n+1)} - \gamma][\ln \frac{1}{\alpha_1 + \beta_1 n'(n'+1)} - \gamma] \right\} \\ &\quad + N\pi^2/6 . \end{aligned} \tag{31}$$

With the expressions of $< S >$ and $< S^2 >$, the predicted deviation ΔS_2 can be derived as

$$\Delta S_2 = \sqrt{< S^2 > - < S >^2} = \sqrt{\frac{\pi^2 N}{6}} . \tag{32}$$

Obviously, we can see that $\Delta S_1 > \Delta S_2$, and the standard fluctuations in both cases are proportional to $\sqrt{N}$, independent of the initial conditions.

REFERENCES

Batchelor, G.K. (1967), *The Theory of Turbulence*. Cambridge University Press, England, 179 pp.

Batchelor, G.K. (1969), Computation of the energy spectrum in homogeneous two–dimensional turbulence, *Phys. Fluid*. Suppl. II, 233–239.

Betchov, R. (1964), Measure of the intricacy of turbulence, *Physics of Fluids*, **7(8):** 1160–1162.

Bourke, W. (1972), An efficient, one–level, primitive–equation spectral model, *Mon. Wea. Rev.*, **100:** 683–689.

Bourke, W., Mcavaney, B., Puri, K. and Thurling, R. (1977), Global modelling of Atmospheric Flow by Spectral Methods, its Method in Computational Physics, **17:** 267–324.

Brachet, M.E., Meneguzzi, M., Politano, H. and Sulen, A.P. (1988), The dynamics of freely decaying two–dimensional turbulence, *J. Fluid Mech.*, **194:** 333–349.

Carnevale, G.F., Frisch, U. and Salmon, R. (1981), H theorems in statistical fluid dynamics, *J. Phys. A*, **14:** 1701–1718.

Carnevale, G.F. (1982), Statistical features of the evolution of two–dimensional turbulence, *J. Fluid Mech.*, **122:** 143–153.

Deem, G.S. and Zabusky, N.J. (1971), Ergodic boundary in numerical simulations of two–dimensional turbulence, *Phys. Rev. Lett.*, **27:** 396–399.

Eliasen, E., Machenhauer, B. and Rasmussen, E. (1970), On a numerical method for integration of hydrodynamical equations with a spectral representation of the horizontal fields, Dept. of Meteorology, Copenhagen University, 35pp.

Fox, D.G. and Orszag, S.A. (1973), Inviscid dynamics of two–dimensional turbulence, *Physics of Fluids*, **16:** 169–171.

Frederiksen, J.S. and Sawford, B.L. (1980), Statistical dynamics of two–dimensional inviscid flow on a sphere, *J. Atmo. Sci.*, **37:** 717–732.

Herring, J.R., Orszag, S.A., Kraichnan, R.H. and Fox, D.G. (1974), Decay of two–dimensional homogeneous turbulence, *J. Fluid Mech.*, **66:** 417–444.

Holloway, G. (1986), Eddies, waves circulation, and mixing: statistical geofluid mechanics, *Ann. Rev. Fluid Mech.*, **18:** 91–147.

Jones, M.N. (1985), *Spherical harmonics and tensors for classical field theory*, (Research Studies Press Ltd.) Appendix 1, England.

Kells, L.C. and Orszag, S.A. (1978), Randomness of low–order models of two–dimensional inviscid dynamics, *Physics of Fluids*, **21:** 162–168.

Kraichnan, R.H. (1967), Inertial ranges in two–dimensional turbulence, *Physics of Fluids*, **10:** 1417–1423.

Kraichnan, R.H. (1975), Statistical dynamics of two–dimensional flow, *J. Fluid Mech.*, **67:** 155–175.

Kraichnan, R.H. and Montgomery, D. (1980), Two–dimensional turbulence, *Rep. Pro. Phys.*, **43:** 547–619.

Lee, T.D. (1952), On some statistical properties of hydrodynamical and magneto– hydrodynamical fields, *Q. Appl. Math.*, **10:** 69–74.

Lilly, D.K. (1969), Numerical simulation of two–dimensional turbulence, *Physics of Fluids*, Suppl. II, 240–249.

Lilly, D.K. (1971), Numerical simulation of developing and decaying two–dimensional turbulence, *J. Fluid. Mech.*, **45:** 395–415.

Orszag, S.A. (1970), Transform method for the calculation of vector–coupled sums: application to the spectral form of the vorticity equation, *J. Atmos. Sci.*, **27:** 890–895.

Orszag, S.A. (1974), Fourier series on sphere, *Mon. Wea. Rev.*, **102:** 56–74.

Seyler, C.E. Jr., Salu, Y., Montgomery, D. and Knorr, G. (1975), Two–dimensional turbulence in inviscid fluids or guiding center plasmas, *Physics of Fluids*, **18:** 803–813.

Shebalin, J.V. (1989), Broken ergodicity and coherent structure in homogeneous turbulence, *Physica D*, **37:** 173–191.

Tang, C.–M. and Orszag, S.A. (1978), Two–dimensional turbulence on the surface of a sphere, *J. Fluid Mech.*, **87:** 305–319.